Correcting in situ chlorophyll fluorescence time-series observations for nonphotochemical quenching and tidal variability reveals nonconservative phytoplankton variability in coastal waters

Luke Carberry [ORCID],[a] Collin Roesler [ORCID],* Susan Drapeau
Earth and Oceanographic Science Department, Bowdoin College, Brunswick, Maine

Abstract

Chlorophyll fluorometry is one of the most commonly implemented approaches for estimating phytoplankton biomass in situ, despite documented sources of natural variability and instrumental uncertainty in the relationship between in vivo fluorescence and chlorophyll concentration. A number of strategies are employed to minimize errors and quantify natural variability in this relationship in the open ocean. However, the assumptions underlying these approaches are unsupported in coastal waters due to the short temporal and small spatial scales of variability, as well as the optical complexity. The largest source of variability in the in situ chlorophyll fluorometric signal is nonphotochemical quenching (NPQ). Typically, unquenched nighttime observations are interpolated over the quenched daytime interval, but this assumes a spatial homogeneity not found in tidally impacted coastal waters. Here, we present a model that provides a tidally resolved correction for NPQ in moored chlorophyll fluorescence measurements. The output of the model is a time series of unquenched chlorophyll fluorescence in tidal endmembers (high and low tide extremes), and thus a time series of phytoplankton biomass growth and loss in these endmember populations. Comparison between modeled and measured unquenched time series yields quantification of nonconservative variations in phytoplankton biomass. Tidally modeled interpolation between these endmember time series yields a highly resolved time series of unquenched daytime chlorophyll fluorescence values at the location of the moored sensor. Such data sets provide a critical opportunity for validating the satellite remotely sensed ocean color chlorophyll concentration data product in coastal waters.

Phytoplankton biomass is governed by dynamic, thermodynamic, and ecological processes that control light availability, nutrient availability, and grazing pressure. Accurately resolving patterns in phytoplankton biomass requires observations made on timescales relevant to these processes, as well as on timescales for which phytoplankton respond physiologically to them. In the open ocean, the temporal and spatial scales of hydrographic variability are long compared to scales of phytoplankton cell growth and division rate (Cloern and Jassby 2010). Thus, coarse resolution Eulerian sampling can be sufficient to resolve relevant changes in phytoplankton biomass, as any observed variations in

phytoplankton biomass are likely due to changes in ecological processes such as phytoplankton physiology or grazing. However, in coastal waters, shelf bathymetry, tides, and currents combine freshwater runoff and oceanic surface and deeper waters over small spatial scales to create considerable spatial complexity in hydrography, mixed layer depth (Simpson et al. 1990), and nutrient content (Townsend et al. 2015), driving spatial complexity in phytoplankton biomass (e.g., Fortunato et al. 2012). Furthermore, short temporal variability, similar in timescale with that of phytoplankton physiological variability, is induced by tidal advection and wind-driven mixing (Cloern et al. 1985; Simpson et al. 1990). This makes deconvolving advectively driven phytoplankton biomass variability from physiologically driven phytoplankton biomass variability difficult in coastal waters using only Eulerian measurements (e.g., Cloern et al. 1989).

In situ validation of remotely sensed chlorophyll concentration in complex coastal waters is also challenged by the optical complexity of coastal waters, where greenness is often driven not just by phytoplankton, but also colored dissolved organic matter and nonalgal particulate material. The time and space scales of variability in coastal waters require in situ observations to be within an hour or less of the midday satellite overpasses to be

*Correspondence: croesler@bowdoin.edu

[a]Present address: Interdepartmental Graduate Program in Marine Science, University of California, Santa Barbara, California

Additional Supporting Information may be found in the online version of this article.

considered a successful matchup (Doerffer and Fischer 1994; Werdell and Bailey 2005; D'Sa et al. 2006; Cui et al. 2010). Therefore, as a result of hydrographic complexity, which complicates measurements of phytoplankton biomass variability, and optical complexity, which complicates remote sensing matchups, fine resolution measurements of phytoplankton biomass, hourly if possible (Li et al. 2010), are essential in coastal waters.

Most techniques to measure phytoplankton biomass, regardless of timescale, use the photosynthetic pigment chlorophyll *a* (Chl *a*) as a proxy, as it is found in all phytoplankton and is unique to photosynthetic primary producers. Caveats exist, however, as the ratio of carbon-to-chlorophyll concentration in phytoplankton cells varies with taxonomy (Chan 1980; Kruskopf and Flynn 2006), photoacclimation (Anning et al. 2000; Moore et al. 2006), and growth phase (Kruskopf and Flynn 2006). The carbon-to-chlorophyll ratio also varies on diel scales as photosynthesis and carbon uptake occur during the day while chlorophyll synthesis occurs at night (Eppley et al. 1971; Sournia 1975). Two sampling approaches exist to measure phytoplankton biomass using Chl *a*: discrete water sampling or in situ observations. Discrete water samples allow for the most accurate quantification of Chl *a* concentration ([Chl *a*]) by using high-pressure liquid chromatography (HPLC; Claustre et al. 2004). However, resolving short temporal variability in phytoplankton biomass using discrete sampling requires either intensive work on behalf of the researcher to collect samples or a method of storing samples; studies using discrete measurements typically employ coarse resolution (as in Cloern et al. 1985) or a short time series (as in Cloern et al. 1989). In situ observations, on the other hand, allow continuous data collection and can be made from any platform, with results obtained in real time. Two common methods of quantifying continuous, in situ phytoplankton biomass, are chlorophyll fluorescence and absorption line height. While absorption line height has shown promising ability to accurately estimate phytoplankton biomass, it requires an in situ spectrophotometer (such as a WETLabs AC meter), which is susceptible to biofouling (Boss et al. 2013; Roesler and Barnard 2013). By contrast, chlorophyll fluorometers are in place on ships, floats, and moorings throughout the world due to their ease of measurement, resistance to biofouling, unambiguous detection of phytoplankton, and relatively robust quantitation.

When chlorophyll molecules absorb light, they emit a small but variable fraction of that light as fluorescence (Huot and Babin 2010). To first order, the intensity of in vivo fluorescence is correlated to [Chl *a*], making chlorophyll fluorescence a useful method of quantifying [Chl *a*] (Lorenzen 1966; Falkowski and Kiefer 1985; Marra and Langdon 1993). Despite the widespread use of chlorophyll fluorometers, the ratio of measured in vivo chlorophyll fluorescence (F_{chl}) to extracted [Chl *a*], called fluorescence yield per chlorophyll, can vary by as much as an order of magnitude over small spatial and temporal scales (Cullen 1982). Phytoplankton taxonomy (Proctor and Roesler 2010), cell size (Alpine and Cloern 1985), pigment packaging (Bricaud et al. 1983, 1995; Sosik et al. 1989; Sosik and Mitchell 1991), and nonphotochemical

quenching (NPQ) (Kiefer 1973; Falkowski and Kolber 1995; Sackmann et al. 2008) all contribute to this variability, making calibration and validation necessary for accurate estimations of [Chl *a*] from F_{chl}. Chlorophyll fluorometers employ a linear calibration constant to relate measured units of fluoresced photons to chlorophyll concentration [Chl *a*], assuming that the fluorescence yield per chlorophyll is constant. Because this assumption is not entirely accurate, further variations in fluorescence yield per chlorophyll must be accounted for (Roesler et al. 2017).

The major challenge for in situ chlorophyll fluorometry is NPQ. NPQ is the process by which phytoplankton cells dissipate excess energy absorbed by photosynthetic pigments (Horton et al. 1996; Huot and Babin 2010). It is a minor de-excitation pathway for phytoplankton cells, halting the transfer of photon energy between light harvesting complexes and Chl *a* molecules in the PSII reaction center when exposed to excess light, thereby diminishing the release of photon energy as fluorescence (Krause and Weis 1991; Horton et al. 1996). Observationally, NPQ manifests as a reduction in measured F_{chl} during the daytime hours (Laney et al. 2005; Roesler and Barnard 2013), with maximal quenching of F_{chl} measurements occurring at noon and at the surface, exponentially decreasing with depth following irradiance (Cullen 1982; Sackmann et al. 2008). Thus, NPQ has significant impacts on in situ fluorometry as a validation product for satellite remote sensing matchups.

Many studies have observed diel reductions in F_{chl} that are attributable to NPQ (Kiefer 1973; Cullen 1982; Falkowski and Kiefer 1985; Marra and Langdon 1993; Falkowski and Kolber 1995; Sackmann et al. 2008; Xing et al. 2012). In regions of the ocean where advectively driven variability in phytoplankton biomass occurs on timescales longer than the diurnal cycle, like the open ocean, conservation of F_{chl} between nighttime measurements can be assumed, allowing the unquenched nighttime observations to be interpolated over the quenched daytime interval (e.g., Li et al. 2010). A different approach used the assumption of F_{chl} uniformity between surface and deep in the mixed layer to create a unique mechanistic model to correct for surface NPQ (Xing et al. 2012). However, if temporal variability in phytoplankton biomass is shorter than the diurnal cycle of NPQ, or if spatial homogeneity cannot be assumed, a robust model that accounts for variations due to advection or heterogeneity is required to retrieve estimates of F_{chl} during NPQ-impacted time intervals.

A common source of short temporal variability phytoplankton biomass in coastal waters is tidal advection (Simpson and Sharples 2012). Chl *a* variability in coastal waters (e.g., the San Francisco Bay) has been shown to be highly correlated with tidal advection (Cloern et al. 1985, 1989; Cloern 1991). Eulerian F_{chl} measurements in tidally impacted waters reveal the signature of two endmembers. The low tide measurement is associated with the upstream (often river) population of phytoplankton and the high tide measurement is associated with the downstream (ocean) population of phytoplankton. The mid-tide F_{chl} measurement is either a conservative mixture of the high and low tide phytoplankton populations, in dynamically dominated systems, or a

nonconservative independent population, either growing, being grazed, or sinking within the estuary. Because the semidiurnal period of tidal advection and the diurnal solar cycle are out of phase, correcting for NPQ by averaging successive nighttime F_{chl} measurements does not accurately represent the daytime measurements in between. Instead, any method of retrieving daytime F_{chl} in tidally impacted regions must take tidal advection into account.

Approaches that accounted for short-term variability driven by tidal advection in the past have used models that assume conservation between high and low tide. One study modeled dissolved oxygen, which, similarly to F_{chl}, has a diel cycle with a different period and phase than the semidiurnal advective cycle of tides (Beck et al. 2015). The advantage of this type of approach is that (1) it separates variability driven by tidal advection from variability internal to the measured variable and (2) it enables identification of periods of nonconservative variability, i.e., when the model and the observations disagree. In the case of F_{chl}, this deconvolves physical variability (i.e., mixing or advection) from biological variability (i.e., blooms and grazing) and reveals the source of nonconservative signals, whether from the low tide up-estuary water, from the mid-tide mid-estuary water, or from the high tide ocean water. Uncovering the causes of conservative or nonconservative behavior in phytoplankton communities is essential to understanding drivers in phytoplankton biomass and community structure in coastal systems.

This article introduces an analytic model for deconvolving semidiurnal tidal cycles and diurnal NPQ cycles to reconstruct robust, high-resolution estimates of chlorophyll concentration from in situ F_{chl} observations in coastal waters. The approach is applicable to moored chlorophyll fluorometers. Ancillary observations of photosynthetically available radiation (PAR) and current velocity reduce uncertainty in the results, but are not required. The goals of this model are to (1) provide robust midday estimates of chlorophyll concentration for constructing ocean color validation data sets and (2) model time series of conservative estimates of phytoplankton biomass in upstream and downstream populations to better quantify nonconservative variations in tidally dominated coastal ecosystems.

Materials and procedures

Study site

Data were collected in Harpswell Sound, Maine, U.S.A. (HS). HS is one of many narrow inlets that comprise Casco Bay (Fig. 1). The long axis of HS is inclined 30° east of true north and a channel runs centrally along the axis. HS lacks a river at its head and the circulation most resembles inverse-estuarine flow, driven by fresh surface water entering the sound from the Kennebec River upstream to its east and compensating high salinity outflow at depth. The sound is generally strongly stratified at the mouth and well mixed at the head where the bathymetry shoals. During intervals of high discharge, the Kennebec River plume is deflected right by Coriolis force and the scale of the Rossby radius directs freshwater flow into HS (Wolovick 2009). During low river
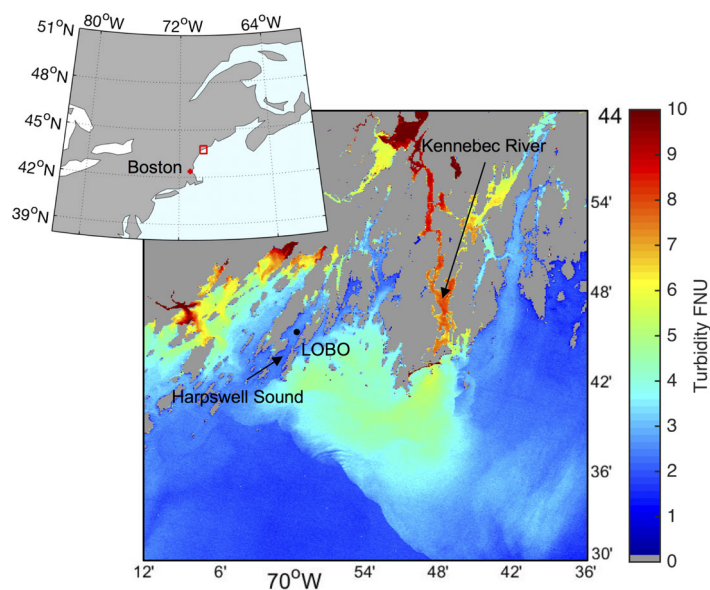

Fig. 1. Landsat image of turbidity in Casco Bay taken on 12 April 2014 (Snyder et al. 2017) showing the deflection of the Kennebec River plume to the mouth of Harpswell Sound. Location of Harpswell Sound, the LOBO mooring site, and the Kennebec River indicated. Red box in inset shows location of Casco Bay relative to the eastern U.S.

discharge, net circulation in HS is negligible but stratification of warm, freshened surface waters overlying deeper, colder, and saltier waters can be mixed by wind events.

Moored data collection

In situ hydrographic observations were made by the Bowdoin Land Ocean Biogeochemical Observatory (LOBO; Sea-Bird Coastal), a floating monitoring platform located at 43°45.70N, 69°59.30W (bowdoin.loboviz.com), deployed annually from March to December since 2014. Temperature and salinity are measured at 1 m by a SBE37-SM C-T recorder (Sea-Bird Electronics). Current velocity profile is measured with an acoustic Doppler current profiler (ADCP; RDI Teledyne) deployed at 1.65 m with 1 m resolution. Hourly F_{chl} is measured with a WETLabs ECO Triplet (BBFL2 model) fluorometer located at 1.5 m, providing excitation at 470 nm and measuring fluorescence response at 695 nm. Multispectral downwelling irradiance (Ed) is measured with a Satlantic, seven channel OCR-507 sensor located at the top of the buoy spar, approximately 2 m above the surface.

Weekly sampling

Weekly sampling trips were conducted via small boat to the LOBO site to collect discrete water samples at 1.5 m, coincident with the in situ fluorometer depth. Triplicate samples were filtered through 25-mm diameter 0.7-μm pore-sized Whatman GF/F filters immediately after collection, placed in 10 mL of 90% HPLC-grade acetone, vortexed to promote extraction, and frozen for 24 h. Samples were centrifuged and extracted [Chl *a*] was determined fluorometrically using a benchtop Turner fluorometer

(Holm-Hansen et al. 1965) that was spectrophotometrically calibrated with chlorophyll *b*-free, purified Chl *a* derived from *Anacystis nidulans* (Sigma Aldrich).

Data processing

Hourly observations obtained from the LOBO consist of the mean of a 60-s burst of 1 Hz sample observations. Factory calibration coefficients are applied to raw observations to obtain geophysical units. Laboratory-derived calibration coefficients for the chlorophyll fluorometers were applied in keeping with the community-established calibration bias of 2 for the WET Labs ECO-series fluorometer (Roesler et al. 2017). Observations compromised by biofouling were removed from the analysis (Roesler 2016). Hourly seven-channel Ed spectra measured on LOBO were normalized by their spectrally integrated value and regressed against a hyperspectral Ed library to estimate hourly hyperspectral Ed. PAR time series was calculated as the definite integral of the hourly hyperspectral Ed from 400 to 700 nm. Northward and eastward components of

current velocity were rotated to the angle of the estuary to produce alongshore velocity.

Sample time series of F_{chl}

Over a 5-week time series in 2016, F_{chl} varied on weekly scales between 1 and 8 μg L^{-1} (Fig. 2A). F_{chl} exhibited daily variations of 100% of the mean over this period. Daily maximal PAR varied from approximately 400 to 2200 μmol q m^{-2} s^{-1} (Fig. 2B). The range in measured current velocity was dominated by alongshore, semidiurnal tidal flow (Fig. 2C). Current velocity range evidenced spring-neap tidal cycles, varying between $\pm$ 0.15 m s^{-1} during neap tide (05/14 first quarter, 05/28 third quarter, and 06/12 first quarter) and $\pm$ 0.3 m s^{-1} during spring tide periods (05/06 new moon, 05/21 full moon, and 06/05 new moon).

F_{chl} exhibited diurnal minima that were concurrent with diurnal increases in PAR intensity (Fig. 2D,E), consistent with NPQ, yet also exhibited variability during nighttime unquenched periods, associated with tidal advection (Fig. 2D,F). For example, over 06/07 to 06/10, nighttime peaks in F_{chl} are concurrent with
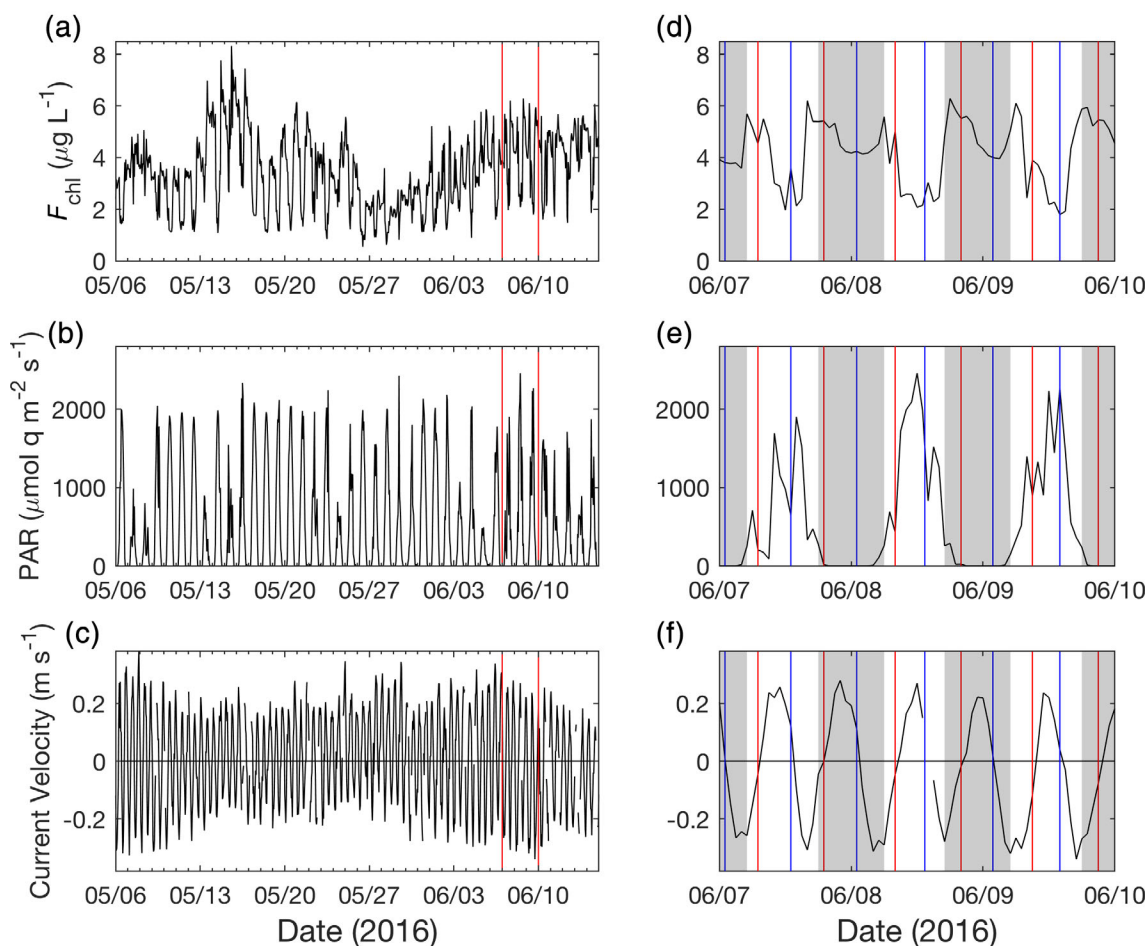

Fig. 2. Six-week (left panels) and 3-d (right panels) time series of hourly observations from the LOBO mooring in 2016: F_{chl} (**A, D**), PAR (**B, E**), and alongshore current velocity measured at 1.5 m (**C, F**). The timing of the 3-d time series is indicated with vertical red lines on the 6-week time series. On the 3-d time series, nighttime intervals indicated by shaded bars, and high and low tide times indicated by blue and red lines, respectively.

low tide (when current velocity transitions from negative to positive; red lines in Fig. 2F), while the nighttime minima are concurrent with high tide (when current velocity transitions from positive to negative; blue lines in Fig. 2F). In this case, it appears that F_{chl} was higher in the upstream water (during low tide at the mooring) than the downstream water (high tide). This example shows that nighttime averaged values represent mixtures of discrete populations and thus averaging adjacent nighttime averages is not an accurate representation of hourly variations in either daytime or nighttime F_{chl} values.

Model development

To quantify the influence of NPQ on F_{chl} observations, incident PAR magnitude is used to identify unquenched F_{chl} measurements. F_{chl} values scaled to their respective nightly maximum value evidenced an onset of quenching at incident PAR values exceeding 350 μmol q m^{-2} s^{-1}, (Fig. 3). The variability in the ratio of raw F_{chl} to nightly maximum F_{chl} at low PAR intensity (i.e., 100–400 μmol q m^{-2} s^{-1}) is due to variability in the raw F_{chl} observations as a result of tidal advection. Ratios that exceed 1 can occur if higher biomass waters are observed in the early morning hours. The increase in the ratio from 0 to 350 μmol q m^{-2} s^{-1} is also potentially a result of decreased photochemical quenching, which occurs as PAR increases and photosynthetic reaction centers close (Morrison 2003; Browning et al. 2014). As PAR approaches 1000 μmol q m^{-2} s^{-1}, NPQ exceeds 50% reduction and manifests as a factor of 2 apparent reduction in daytime phytoplankton biomass in real time observations. In the absence of PAR observations, time of day can also be used as a proxy for PAR. Scaling F_{chl} to maximal F_{chl} occurring between 18:00 and 06:00 h (1 h before sunset to
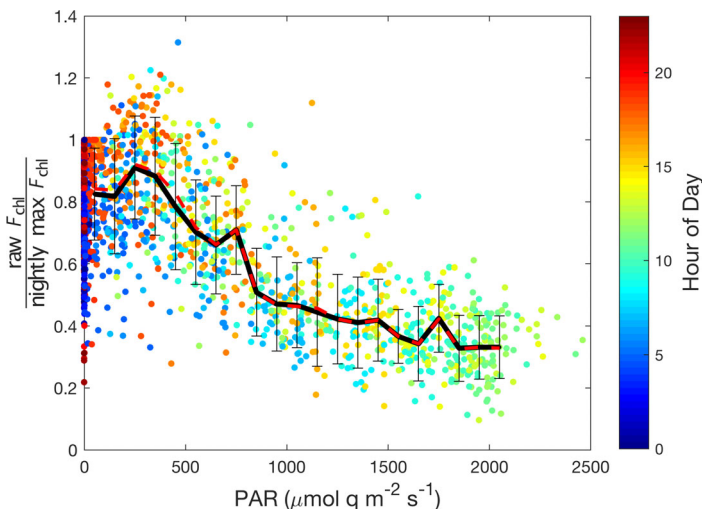

Fig. 3. Hourly F_{chl} observations, scaled to the nightly maximal F_{chl} occurring below PAR values of 100 μmol q m^{-2} s^{-1}, as a function of incident PAR. Symbols colored by hour of day. Median and standard deviation F_{chl} values shown by solid black line and error bars, respectively, at PAR intervals of 100 μmol q m^{-2} s^{-1}. F_{chl} scaled to max F_{chl} observed between 1800 and 0600 is indistinguishable from F_{chl} scaled by max F_{chl} below 100 μmol q m^{-2} s^{-1}, with median values shown by dashed red line and error bars similar in size to F_{chl} scaled by max F_{chl} below 100 μmol q m^{-2} s^{-1} (not shown).

1 h after sunrise) is more conservative than using PAR, as it does not include specific observations between dawn and dusk that had low PAR due to clouds, but yields statistically identical results over the time series (Fig. 3, dashed red line). Given that scaled F_{chl} values increase slightly from 0 and 400 μmol q m^{-2} s^{-1}, particularly between 300 and 400 μmol q m^{-2} s^{-1}, we use 300 μmol q m^{-2} s^{-1} as the threshold for NPQ onset. All F_{chl} measurements observed at lower PAR values are considered unquenched (Matlab functions to apply the model can be found in Supporting Information).

The threshold for NPQ is used to create a subset time series of unquenched hourly F_{chl} observations (Fig. 4A). The gap between quenched and unquenched observations confirms that the onset of quenching is rapid, rather than gradual, as there are few middle values between the two subsets of raw observations. Two separate subsets of the observations are created alongside this one based upon the timing of high and low tide. These are identified from current velocity observations using the following criteria (Fig. 4B):

$$\text{High tide}: V_a = 0; \text{ and } dV_a/dt < 0 \qquad (1a)$$

$$\text{Low tide}: V_a = 0; \text{ and } dV_a/dt > 0 \qquad (1b)$$

where V_a is the observed alongshore velocity time series at 1.5 m in the estuary. In the absence of concurrent current velocity measurements, high and low tide times can be identified from a local tide chart or generated from a tidal model based on a sample current velocity data set (e.g., U-tide, Codiga 2011). The intersection of each of the two tidal maxima subsets with the unquenched subset forms a set with elements of unquenched high tide F_{chl} and a set with elements of unquenched low tide F_{chl} (Fig. 4C). These two sets are the unquenched high tide and low tide conservative endmembers of F_{chl} in the estuary representing upstream and downstream populations, and together they create a range envelope.

The phasing between semidiurnal (or diurnal) tides and diurnal quenching (e.g., approximately 24 h, 48 min vs. 24 h) yields an unevenly spaced time series with days for which there are either no unquenched high tide or no unquenched low tide F_{chl} measurements. To account for this discrepancy, missing high or low tide F_{chl} measurements are estimated by linear interpolation between measured, unquenched successive high tide or low tide F_{chl} measurements, making a time series of unquenched F_{chl} observations at every high and low tide (Fig. 5A). The underlying assumption is that within a single endmember water mass, the time evolution of phytoplankton biomass is slower than changes observed at the stationary buoy (Lagrangian vs. Eulerian, respectively).

A cosinusoidal model representing tidal advection is used to calculate hourly unquenched F_{chl} piecewise between each high and low tide endmember (Fig. 5B):

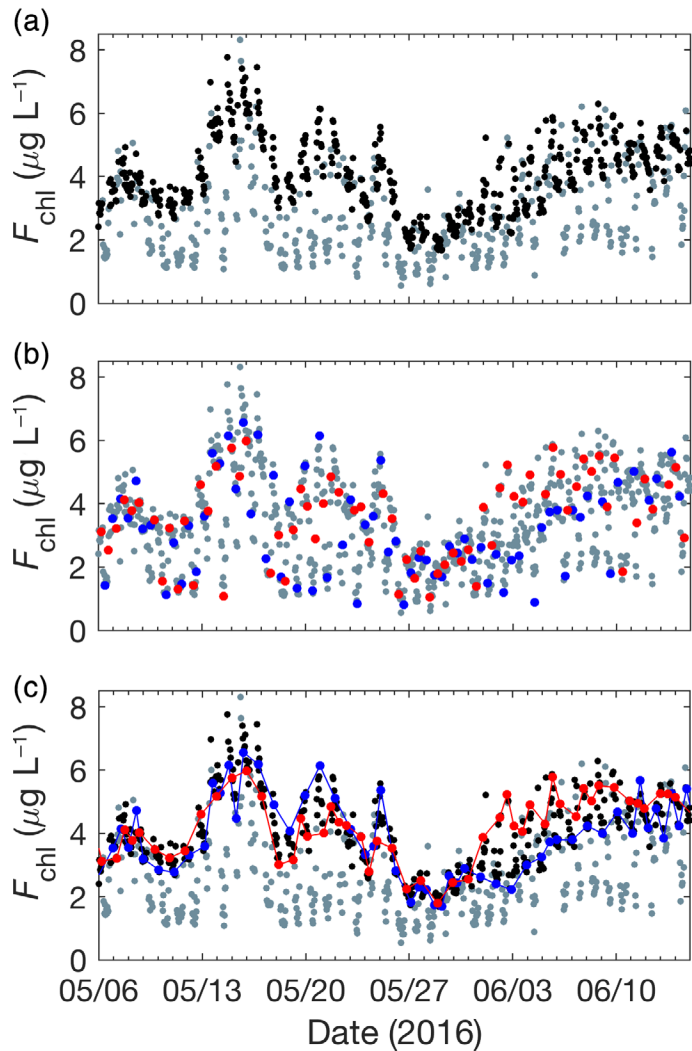$$F_{chl}(t) = -A \times \left(\cos\left(\pi \times \frac{t - t_1}{t_2 - t_1} \right) \right) + O \qquad (2)$$

Fig. 4. Six-week time series of hourly raw in situ F_{chl} observations (gray symbols) and F_{chl} observations (**A**) coincident with PAR < 300 μmol q m^{-2} s^{-1} (black symbols), (**B**) coincident with high tide and low tide (blue and red symbols, respectively) and (**C**) co-occurring unquenched (from **A**) and high and low tide (from **B**). Blue and red lines in (**C**) provide approximate time series of high and low tide endmember values, respectively.

where t is time between t_1, time of the present tidal maxima, and t_2, time of the next tidal maxima; A is the amplitude in F_{chl} between t_1 and t_2; $\cos\left(\pi \times \frac{t-t_1}{t_2-t_1}\right)$ sets the phase of cosine interpolation using the ratio of time elapsed ($t-t_1$) to the total time in the interval (t_2-t_1); and O is the offset of the cosine interpolation from the x axis, calculated as the midpoint between F_{chl} (t_1) and F_{chl} (t_2). The model output is the hourly time series of unquenched, tidally resolved F_{chl} (Fig. 5B; referred to as "corrected" below).

Assessment

As part of our model assessment, we identify and quantify the effects of both tidal advection and NPQ on measurements
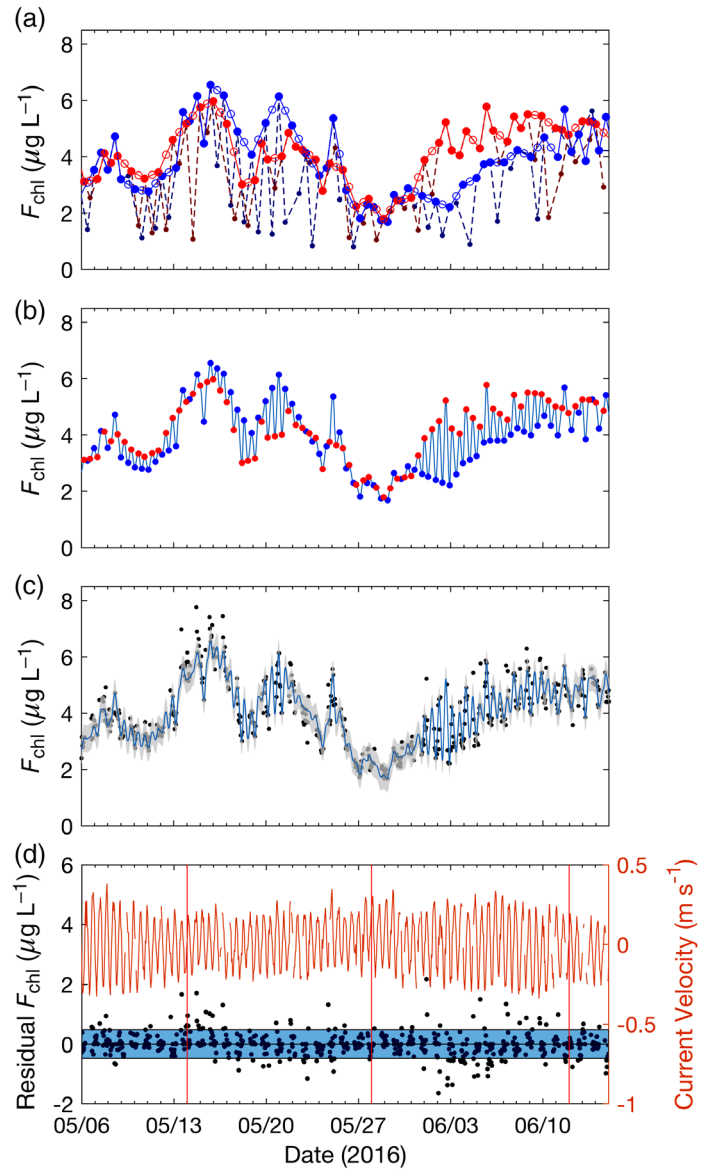
Fig. 5. Six-week time series of (**A**) measured F_{chl} at high tide and low tide (filled symbols, blue and red, respectively) with modeled daytime values (open symbols), and quenched raw daytime observations at high and low tides (dark blue and red dots connected to unquenched observations with dashed lines; (**B**) modeled hourly, unquenched, tidally corrected F_{chl} time series (blue line), calculated using a cosine function (Eqn. 2) fit to observed and interpolated occurrences of unquenched F_{chl} at high and low tide times in (**A**); (**C**) hourly modeled F_{chl} time series from (**B**) (blue line, RMSE error envelope in gray) with hourly unquenched F_{chl} observations from Fig. 4A; and (**D**) residual nighttime F_{chl} (raw minus model; black symbols) and RMSE envelope (blue band, $\pm$ 0.34 mg L^{-1}) with alongshore current velocity (m s^{-1}). Red vertical lines indicate timing of neap tide.

of F_{chl}. The model incorporates both the NPQ and tidal factors into its correction and thus it is difficult to separate them during the day. However, at night, when NPQ is not occurring, the effect of tidal advection can be isolated. The observed

variability in F_{chl} due to tidal advection, while not negligible, is small compared to that due to NPQ (Fig. 2D). Therefore, the corrected F_{chl} should not differ significantly from the observed F_{chl} for nighttime values and indeed it does not ($m = 0.87 \pm 0.025$, $b = 0.53$, root mean square error (RMSE) = 0.48; Fig. 6A). Because the model assumes conservative variability between tidal maxima, the spread about this relationship reveals the nonconservative variability in F_{chl} in the estuary (a combined model using the raw, unquenched data during the nighttime and modeled F_{chl} during the day would show the blue and red points in Fig. 6A all falling on the 1:1 line). Nonconservative variability can be clearly seen in the mean ratio of raw F_{chl} to corrected F_{chl}, as a function of hour of day (Fig. 6B), where the error bars provide an estimate of the range of nonconservative variations in F_{chl} at the level of approximately $\pm 10\%$. During the daytime hours of NPQ, this ratio drops from 1 to 0.6 with a range of $\pm 30\%$, encapsulating both natural variations in NPQ, due to variations in PAR intensity, and nonconservative variations in F_{chl}. If the nonconservative variations observed during the daytime are comparable to those at night, these results would suggest that *variations* in NPQ are approximately $\pm 20\%$ throughout the daytime (i.e., maximally quenched at noon by up to 40% on average but with 20% variability in the degree of NPQ). Thus, tidal advection drives about 10% of variability and NPQ drives 20% of the variability in the correction.

Next, we examine the model's effectiveness in (1) correcting nonphotochemically quenched observations and (2) correcting for tidal advection.

(1) The ratio of raw quenched F_{chl} measurements to corrected values ranges from 30% to as high as 90%. Thus, the model makes considerable corrections to raw daytime F_{chl} observations. Raw daytime F_{chl} observations are increased by between 1 and 5 μg L^{-1}

once corrected by the model (midday observations; Fig. 6A), which accounts for the wide spread of daytime points about the 1:1 line ($m = 0.47 \pm 0.036$, $b = 2.62$, RMSE = 1.61). Just as we used hourly F_{chl} observations scaled to maximal nighttime F_{chl} as a function of PAR to assess irradiance threshold for NPQ, a similar analysis performed with corrected F_{chl} should not have a dependence upon incident irradiance (Fig. 6C). The ratio is clearly invariant over the entire range of PAR ($m = 0.00 \pm 0.00$, $p = 0.81$) and the variability is on the order of $\pm 10\%$, associated with nonconservative variability. What this means is that rather than removing nearly 12 h's worth of the hourly observations (i.e., all of the daytime observations), we have recovered them. This result is a critical achievement not only increasing the temporal resolution of coastal F_{chl} measurements, but also providing a mechanism for using in situ F_{chl} for satellite validation of the ocean color chlorophyll data product.

(2) We assess the utility of the model in correcting for tidal advection by first comparing it to two conventional approaches for dealing with NPQ (interpolating linearly from dusk to dawn and interpolating between nighttime averaged observations) and second by evaluating the time series of tidal maxima endmember F_{chl}, before and after correction, for ecological realism. Conventional approaches for daytime interpolation do not account for the daytime variability in F_{chl} caused by variation in the phytoplankton biomass of tidal endmembers nor the advective variation between endmembers, and thus do not provide a robust estimate of F_{chl} during the daytime (Fig. 7A). The histogram of the ratio of raw nighttime F_{chl} to nightly mean F_{chl} demonstrates the degree of variability that exists due to variation between tidal endmembers (essentially a histogram of the data in Figs. 6C, 7B). Variability averages $\pm 10\%$ but can be as high as 50% in some instances, none of which is accounted for by conventional approaches. In the uncorrected F_{chl} endmembers, F_{chl} grows and
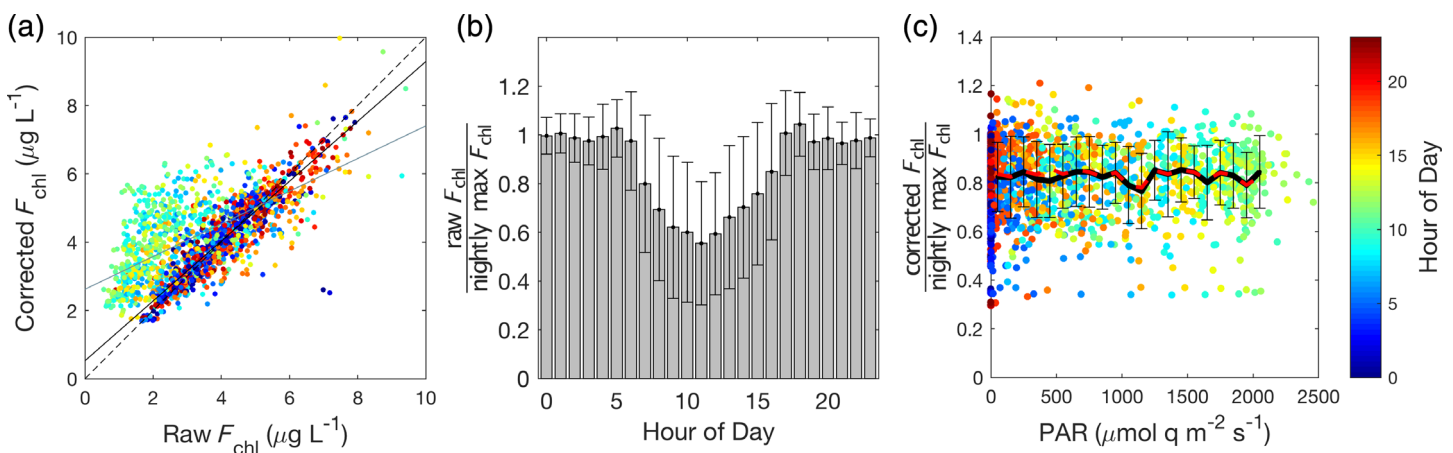

Fig. 6. (**A**) Corrected F_{chl} vs. raw F_{chl} for the period 29 April 2016–12 July 2016, color-coded by hour of the day. Line of best fit plotted for nighttime observations (19:00–05:00 h local time) in black ($m = 0.87 \pm 0.025$, $b = 0.53$, RMSE = 0.48) and for daytime observations (06:00–18:00 h local time) in gray ($m = 0.47 \pm 0.036$, $b = 2.62$, RMSE = 1.61). Dashed line shows 1:1 relationship. (**B**) Ratio of raw F_{chl} to corrected F_{chl} binned by local hour of day over the period 29 April 2016–12 July 2016, with standard deviation error bars. (**C**) Corrected F_{chl} normalized to nightly maximal value of F_{chl} vs. PAR, color-coded by hour of day (as in Fig. 3). Black line represents mean values over 100 μmol q m^{-2} s^{-1} bins, with standard deviation error bars, while dashed red line represents mean values between 18:00 and 06:00 h.
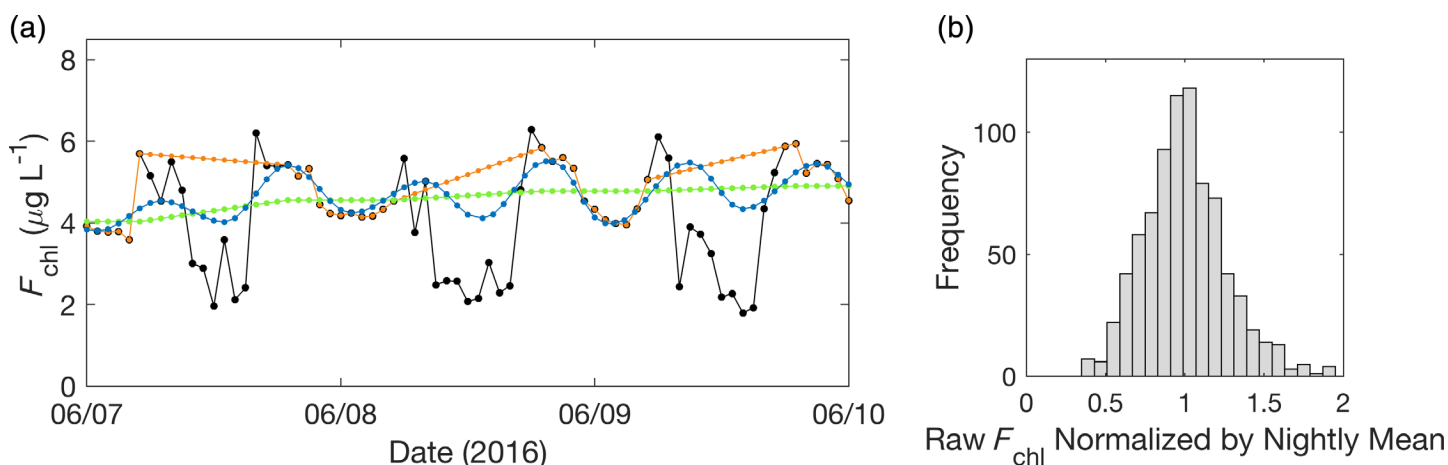
Fig. 7. (**A**) Three-day time series of raw calibrated F_{chl} (black) with three F_{chl} daytime corrections. Blue line indicates tidal model, orange line indicates dawn to dusk interpolation, and green line indicates the nighttime average interpolation. (**B**) Histogram of raw nighttime F_{chl} measurements normalized to the nightly mean value.

declines at unrealistic rates (e.g., on 05/20 in the high tide endmember, it exhibits multiple apparent changes of order factor of 2–3 within 24 h; Fig. 5A). In the corrected endmembers, by contrast, F_{chl} exhibits growth rates of 0.2–0.3 d^{-1} during periods of growth, comparable to temperate phytoplankton globally (Calbet and Landry 2004), and blooms that endure on timescales of weeks (Fig. 5A). Thus, the model reveals ecologically relevant variability in F_{chl}. Individual growth rates of the F_{chl} endmembers can thus be quantified, something that would not be possible from the raw F_{chl} observations. For example, following a period of uniformity, low tide and high tide populations diverge on 5/27, with low tide F_{chl} increasing at a rate of 0.89 μg L^{-1} d^{-1} for 3 d, while high tide F_{chl} lags for 3 d before increasing by 0.50 μg L^{-1} d^{-1} over the next 3 d (Fig. 5B).

Identifying nonconservative mixing

The model provides an estimate of hourly F_{chl} that would be observed assuming conservative mixing between the high and low tide endmember populations. Against the conservative mixing assumption, intervals of nonconservative mixing can be identified and quantified from the perspective of phytoplankton growth and loss. At times, nonconservative growth occurs within the tidal range of the mooring, for example, from 05/13 to 05/16, where residual F_{chl} is higher than both adjacent high tide and low tide F_{chl} values (Fig. 5C,D). At other times, nonconservative loss appears to occur within the tidal range of the mooring, with raw, nighttime F_{chl} below adjacent F_{chl} at high or low tide, for example, from 06/01 to 06/07. Such mid-tide growth and loss would not be visible without the correction scheme provided by the model, and it appears that the residuals are not randomly distributed. More extensive analysis of F_{chl} nonconservative residuals would likely reveal a relationship between tidal dynamics and phytoplankton dynamics that has been demonstrated in other

estuaries (Balch 1981; Cloern 1991; Cadier et al. 2017) and in modeling (Sharples 2007).

Extracted chlorophyll matchup

Finally, we compare F_{chl} to extracted [Chl a], which allows an estimation of the model's absolute accuracy. A weak linear relationship was observed between raw F_{chl} and extracted [Chl] (RMSE = 2.03, Fig. 8A). In contrast, a much stronger linear relationship emerged between the corrected F_{chl} and extracted [Chl a] (RMSE = 1.03, Fig. 8B). Point by point matchups with extracted [Chl a] are challenging for all of the reasons that calibrating a fluorometer is challenging: taxonomy, light history, and growth phase (e.g., Roesler et al. 2017). However, taken together, the model reduces the error in the matchup by roughly a factor of 2.

Discussion and outlook

The model presented here provides a means for obtaining daytime estimates of chlorophyll fluorescence, a proxy for phytoplankton biomass, in tidally impacted regions from in situ chlorophyll fluorescence by using the periodicity of tidal advection to estimate unquenched daytime values. By accounting for the presence of two phytoplankton populations associated with the maximum extents of high and low tide, hourly time-series observations at a single location, amid tidal fluctuation, yield independent assessment of both populations. In other words, the method enables a study of coastal phytoplankton biomass dynamics in a Lagrangian sense from Eulerian measurements. The assumption of conservative mixing inherent in the model additionally provides the advective context against which unquenched F_{chl} observations can be examined to reveal nonconservative behavior in F_{chl} that would not be resolved with other interpolation schemes. Similarly, deconvolving the diurnal cycle of NPQ from the semidiurnal cycle of tidal advection enables the study of photoacclimation, trophic status, and community
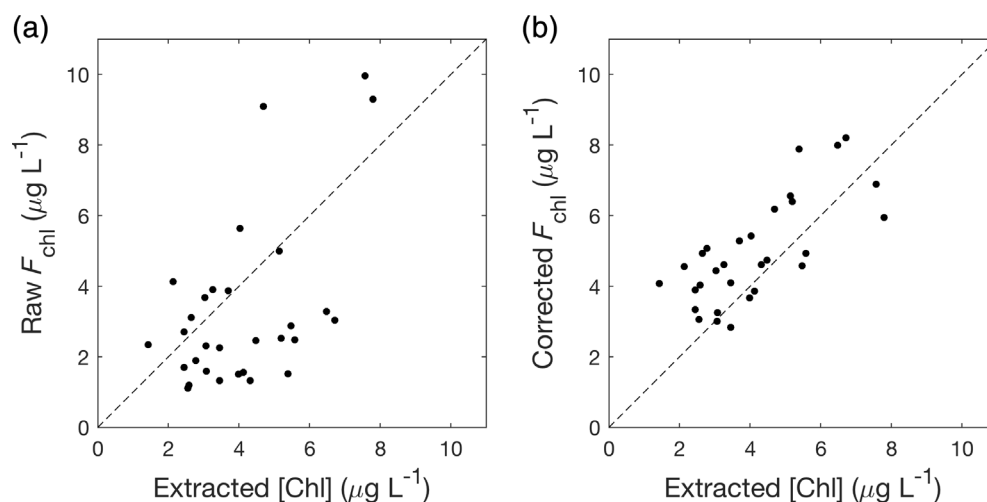
Fig. 8. Raw (**A**) and corrected (**B**) F_{chl} vs. extracted [Chl] from spring and summer 2015–2017 in HS. Dashed line shows 1:1 relationship. RMSE is 2.03 for raw F_{chl} and 1.03 for corrected F_{chl}.

structure influences on NPQ. No traditional method of correcting F_{chl} for NPQ is as robust in coastal, tidally impacted waters.

The model is suitable for any coastally moored chlorophyll fluorometer and has applications in ecosystem monitoring and ocean color sensor validation. It is necessary for F_{chl} measurements made in tidally impacted waters, where distinguishing phytoplankton biomass variability driven by tidal advection from phytoplankton biomass variability driven by phytoplankton physiology is otherwise difficult. When applied to estuaries, the method allows for the monitoring of true growth and decay of both ocean and river populations of phytoplankton, making it ideal for coastal ecosystem management. Otherwise, the effect of tidal advection on F_{chl} would appear as short temporal variability in coastal ecosystems (as in Cloern et al. 1989). The model is also useful for remote sensing matchup contexts, where achieving in situ validation of satellite ocean color sensors is challenging (Werdell and Bailey 2005), and requires daily midday measurements of phytoplankton biomass. This is especially difficult in coastal waters, where input source variability creates significant spatial and temporal variability in optical components of the water column (Sauer and Roesler 2013) and where tidal advection complicates traditional methods of NPQ correction. Thus, this model is ideal for remote sensing and ecosystem monitoring applications as it can accurately monitor both river and ocean phytoplankton populations with just one sensor and provide a robust estimate of F_{chl} without the artifact of NPQ, coincident with satellite overpass.

Understanding the drivers of coastal phytoplankton growth, particularly in the Gulf of Maine, is a continually evolving question, and one that has not yet been convincingly answered. This is likely due to the complexity of the coastline, the significant tidal range, the distributed river system that produces buoyantly driven coastal currents (Pettigrew et al. 2005), and the variability in deep-water input (Townsend et al. 2015). In addition to its

utility for coastal monitoring and remote sensing, the model has the potential to help answer this question, particularly concerning source of phytoplankton blooms throughout the year and the relationship between tidal dynamics and phytoplankton productivity. The formation of phytoplankton blooms is complicated by coastal water mass mixing and tidal advection, and the ability to track growing and decaying phytoplankton populations as they are advected into and out of estuaries is an important step in understanding them. Specifically, harmful algal blooms, dominated by *Alexandrium fundyense* in the Gulf of Maine, involve a mechanism of ocean-ward and shoal-ward transport (McGillicuddy et al. 2003), and tracking known *Alexandrium* populations in both archived F_{chl} data and future data collection will assist in understanding their behavior. Thanks to an initial investment by the National Oceanographic Partnership Program (NOPP), chlorophyll fluorometers, ADCPs, and (in some cases) PAR sensors are already in place throughout the Gulf of Maine on the Northeastern Regional Association of Coastal Ocean Observing Systems (NERACOOS) buoy array, making the Gulf of Maine an ideal first location for application of this model.

In addition to aiding in understanding how and where phytoplankton populations bloom, this model can reveal how those populations respond to changes in the dynamic and thermodynamic forcings that affect phytoplankton growth, one of which is spring-neap tidal forcing. The spring-neap tidal cycle affects nutrient content and mixed layer depth in estuaries through tidal stirring (Cloern 1991; Simpson and Sharples 2012). Fortnightly spring-neap tidal variations in tidal energy and range lead to increased spring tide stirring and decreased neap tide stirring. Phytoplankton blooms are found to be coherent with both the spring tide (Balch 1981) and the neap tide (Cloern 1991; Sharples et al. 2006; Cadier et al. 2017) depending upon whether they are nutrient or light-limited. By

highlighting periods of nonconservative behavior in phytoplankton biomass, the model is suited to reveal the effect of the spring-neap tidal cycle on coastal phytoplankton growth and cell division demonstrated theoretically (Sharples 2007).

In light of the complexity in physical drivers of phytoplankton biomass dynamics, the model presented here provides a pathway forward to identifying distinct phytoplankton populations within embayments from a single moored chlorophyll fluorometer. Furthermore, it enables quantification of growth rates of these populations and identification of nonconservative behavior, all three of which are critical to understanding the drivers of phytoplankton biomass dynamics and will lead to important discoveries in the future.

Comments and recommendations

This model requires concurrent measurements of current velocity, PAR, and F_{chl}. However, it can be parameterized without explicit current and/or PAR measurements. At its simplest, the model requires only a chlorophyll fluorometer and a tide chart. In the absence of a PAR sensor, nonphotochemically quenched F_{chl} observations can be identified by time of day, rather than by PAR, which increases the absolute error compared to extracted [Chl *a*] slightly (*see* Fig. 3; RMSE = 1.13 vs. RMSE = 1.03 for the full model). The most robust approach to selecting unquenched values using hour of day is to calculate the interval 1 h pre-dusk through 1 h post-dawn using a simple seasonal insolation-by-latitude model. In the absence of an ADCP or current meter, tide chart predictions of high and low tide can be used to create F_{chl} high and low tide endmembers. Alternatively, a theoretical model of dynamic tides, U-tide, can be used, if a sample current velocity data set from the desired location is available (Codiga 2011). If current velocity is not used, residuals identified by the model will include nontidal advection in addition to nonconservative variability in phytoplankton biomass, complicating the identification of nonconservative behavior. As expected, error is higher if no ADCP is available (RMSE = 1.44; U-tide used to identify tidal maxima). Finally, if time of day is used instead of PAR, and U-tide is used instead of current velocity observations, error similarly increases compared to the full model (RMSE = 1.25). PAR and current velocity serve only to select unquenched measurements and identify high and low tide times, respectively. Once this is done, the steps defined in "Model development" section are the same. The model is thus suitable for a range of instrumental capabilities while still regaining its primary function of correcting F_{chl} for NPQ and tidal advection if only a chlorophyll fluorometer and a tide chart are available.

References

Alpine, A. E., and J. E. Cloern. 1985. Differences in in vivo fluorescence yield between three phytoplankton size classes. J. Plankton Res. **7**: 381–390. doi:10.1093/plankt/7.3.381

Anning, T., H. L. MacIntyre, S. M. Pratt, P. J. Sammes, S. Gibb, and R. J. Geider. 2000. Photoacclimation in the marine diatom *Skeletonema costatum*. Limnol. Oceanogr. **45**: 1807–1817. doi:10.4319/lo.2000.45.8.1807

Balch, W. M. 1981. An apparent lunar tidal cycle of phytoplankton blooming and community succession in the Gulf of Maine. J. Exp. Mar. Biol. Ecol. **55**: 65–77. doi:10.1016/0022-0981(81)90093-9

Beck, M. W., J. D. Hagy, and M. C. Murrell. 2015. Improving estimates of ecosystem metabolism by reducing effects of tidal advection on dissolved oxygen time series. Limnol. Oceanogr.: Methods **13**: 731–745. doi:10.1002/lom3.10062

Boss, E., and others. 2013. The characteristics of particulate absorption, scattering and attenuation coefficients in the surface ocean; contribution of the Tara oceans expedition. Methods Oceanogr. **7**: 52–62. doi:10.1016/j.mio.2013.11.002

Bricaud, A., A. Morel, and L. Prieur. 1983. Optical efficiency factors of some phytoplankters. Limnol. Oceanogr. **28**: 816–832. doi:10.4319/lo.1983.28.5.0816

Bricaud, A., M. Babin, A. Morel, and H. Claustre. 1995. Variability in the chlorophyll-specific absorption coefficients of natural phytoplankton: Analysis and parameterization. J. Geophys. Res. Oceans **100**: 13321–13332. doi:10.1029/95JC00463

Browning, T., H. Bouman, and C. Moore. 2014. Satellite-detected fluorescence: Decoupling nonphotochemical quenching from iron stress signals in the South Atlantic and Southern Ocean. Global Biogeochem. Cycles **28**: 510–524. doi:10.1002/2013GB004773

Cadier, M., T. Gorgues, S. LHelguen, M. Sourisseau, and L. Memery. 2017. Tidal cycle control of biogeochemical and ecological properties of a macrotidal ecosystem. Geophys. Res. Lett. **44**: 8453–8462. doi:10.1002/2017GL074173

Calbet, A., and M. Landry. 2004. Phytoplankton growth, microzooplankton grazing, and carbon cycling in marine systems. Limnol. Oceanogr. **49**: 51–57. doi:10.4319/lo.2004.49.1.0051

Chan, A. T. 1980. Comparative physiological study of marine diatoms and dinoflagellates in relation to irradiance and cell size. II. Relationship between photosynthesis, growth, and carbon/chlorophyll a ratio. J. Phycol. **16**: 428–432. doi:10.1111/j.1529-8817.1980.tb03056.x

Claustre, H., and others. 2004. An intercomparison of HPLC phytoplankton pigment methods using in situ samples: Application to remote sensing and database activities. Mar. Chem. **85**: 41–61. doi:10.1016/j.marchem.2003.09.002

Cloern, J. E. 1991. Tidal stirring and phytoplankton bloom dynamics in an estuary. J. Mar. Res. **49**: 203–221. doi:10.1357/002224091784968611

Cloern, J. E., B. E. Cole, R. L. Wong, and A. E. Alpine. 1985. Temporal dynamics of estuarine phytoplankton: A case study of

San Francisco Bay, p. 153–176. *In* Temporal dynamics of an estuary. Springer. doi:10.1007/BF00048693

Cloern, J. E., T. M. Powell, and L. M. Huzzey. 1989. Spatial and temporal variability in South San Francisco Bay (USA). II. Temporal changes in salinity, suspended sediments, and phytoplankton biomass and productivity over tidal time scales. Estuar. Coast. Shelf Sci. **28**: 599–613. doi:10.1016/0272-7714(89)90049-8

Cloern, J. E., and A. D. Jassby. 2010. Patterns and scales of phytoplankton variability in estuarine–coastal ecosystems. Estuaries Coast. **33**: 230–241. doi:10.1007/s12237-009-9195-3

Codiga, D. L. 2011. Unified tidal analysis and prediction using the UTide Matlab functions. Graduate School of Oceanography, Univ. of Rhode Island. ftp://www.po.gso.uri.edu/pub/downloads/codiga/pubs/2011Codiga-UTide-Report.pdf

Cui, T., J. Zhang, S. Groom, L. Sun, T. Smyth, and S. Sathyendranath. 2010. Validation of MERIS ocean-color products in the Bohai Sea: A case study for turbid coastal waters. Remote Sens. Environ. **114**: 2326–2336. doi:10.1016/j.rse.2010.05.009

Cullen, J. J. 1982. The deep chlorophyll maximum: Comparing vertical profiles of chlorophyll a. Can. J. Fish. Aquat. Sci. **39**: 791–803. doi:10.1139/f82-108

Doerffer, R., and J. Fischer. 1994. Concentrations of chlorophyll, suspended matter, and gelbstoff in case II waters derived from satellite coastal zone color scanner data with inverse modeling methods. J. Geophys. Res. Oceans **99**: 7457–7466. doi:10.1029/93JC02523

D'Sa, E. J., R. L. Miller, and C. Del Castillo. 2006. Bio-optical properties and ocean color algorithms for coastal waters influenced by the Mississippi River during a cold front. Appl. Opt. **45**: 7410–7428. doi:10.1364/AO.45.007410

Eppley, R. W., J. N. Rogers, J. J. McCarthy, and A. Sournia. 1971. Light/dark periodicity in nitrogen assimilation of the marine phytoplankters skeletonema costatum and *Coccolithus huxleyi* in n-limited chemostat culture. J. Phycol. **7**: 150–154. doi:10.1111/j.1529-8817.1971.tb01494.x

Falkowski, P., and D. A. Kiefer. 1985. Chlorophyll a fluorescence in phytoplankton: Relationship to photosynthesis and biomass. J. Plankton Res. **7**: 715–731. doi:10.1093/plankt/7.5.715

Falkowski, P., and Z. Kolber. 1995. Variations in chlorophyll fluorescence yields in phytoplankton in the world oceans. Funct. Plant Biol. **22**: 341–355. doi:10.1071/PP9950341

Fortunato, C. S., L. Herfort, P. Zuber, A. M. Baptista, and B. C. Crump. 2012. Spatial variability overwhelms seasonal patterns in bacterioplankton communities across a river to ocean gradient. ISME J. **6**: 554–563. doi:10.1038/ismej.2011.135

Holm-Hansen, O., C. J. Lorenzen, R. W. Holmes, and J. D. Strickland. 1965. Fluorometric determination of chlorophyll. ICES J. Mar. Sci. **30**: 3–15. doi:10.1093/icesjms/30.1.3

Horton, P., A. Ruban, and R. Walters. 1996. Regulation of light harvesting in green plants. Annu. Rev. Plant Biol. **47**: 655–684. doi:10.1146/annurev.arplant.47.1.655

Huot, Y., and M. Babin. 2010. Overview of fluorescence protocols: Theory, basic concepts, and practice, p. 31–74. *In* D. J. Suggett, M. A. Borowitzka and O. Prášil [eds.], Chlorophyll a fluorescence in aquatic sciences: Methods and applications. Springer. doi:10.1007/978-90-481-9268-7

Kiefer, D. 1973. Fluorescence properties of natural phytoplankton populations. Mar. Biol. **22**: 263–269. doi:10.1007/BF00389180

Krause, G., and E. Weis. 1991. Chlorophyll fluorescence and photosynthesis: The basics. Annu. Rev. Plant Biol. **42**: 313–349. doi:10.1146/annurev.pp.42.060191.001525

Kruskopf, M., and K. J. Flynn. 2006. Chlorophyll content and fluorescence responses cannot be used to gauge reliably phytoplankton biomass, nutrient status or growth rate. New Phytol. **169**: 525–536. doi:10.1111/j.1469-8137.2005.01601.x

Laney, S. R., R. M. Letelier, and M. R. Abbott. 2005. Parameterizing the natural fluorescence kinetics of *Thalassiosira weissflogii*. Limnol. Oceanogr. **50**: 1499–1510. doi:10.4319/lo.2005.50.5.1499

Li, W. K., M. R. Lewis, and W. G. Harrison. 2010. Multiscalarity of the nutrient–chlorophyll relationship in coastal phytoplankton. Estuaries Coast. **33**: 440–447. doi:10.1007/s12237-008-9119-7

Lorenzen, C. J. 1966. A method for the continuous measurement of in vivo chlorophyll concentration, p. 223–227. *In* Deep sea research and oceanographic abstracts. Elsevier. doi:10.1016/0011-7471(66)91102-8

Marra, J., and C. Langdon. 1993. An evaluation of an in situ fluorometer for the estimation of chlorophyll a. Lamont-Doherty Earth Observatory Tech. Rep. LDEO-93-1.

McGillicuddy, D., Jr., and others. 2003. A mechanism for offshore initiation of harmful algal blooms in the coastal Gulf of Maine. J. Plankton Res. **25**: 1131–1138. doi:10.1093/plankt/25.9.1131

Moore, C. M., and others. 2006. Phytoplankton photoacclimation and photoadaptation in response to environmental gradients in a shelf sea. Limnol. Oceanogr. **51**: 936–949. doi:10.4319/lo.2006.51.2.0936

Morrison, J. R. 2003. In situ determination of the quantum yield of phytoplankton chlorophyll a fluorescence: A simple algorithm, observations, and a model. Limnol. Oceanogr. **48**: 618–631. doi:10.4319/lo.2003.48.2.0618

Pettigrew, N. R., and others. 2005. The kinematic and hydrographic structure of the Gulf of Maine Coastal Current. Deep-Sea Res. Part II Top. Stud. Oceanogr. **52**: 2369–2391. doi:10.1016/j.dsr2.2005.06.033

Proctor, C. W., and C. S. Roesler. 2010. New insights on obtaining phytoplankton concentration and composition from in situ multispectral chlorophyll fluorescence. Limnol.

Oceanogr.: Methods **8**: 695–708. doi:10.4319/lom.2010.8.0695

Roesler, C., and others. 2017. Recommendations for obtaining unbiased chlorophyll estimates from in situ chlorophyll fluorometers: A global analysis of WET Labs ECO sensors. Limnol. Oceanogr.: Methods **15**: 572–585. doi:10.1002/lom3.10185

Roesler, C. S. 2016. In situ chlorophyll fluorescence observations on NERACOOS Mooring A01: Revised data flagging and changing phenology, p. 11. Report 2016-15. Boston: Massachusetts Water Resources Authority.

Roesler, C. S., and A. H. Barnard. 2013. Optical proxy for phytoplankton biomass in the absence of photophysiology: Rethinking the absorption line height. Methods Oceanogr. **7**: 79–94. doi:10.1016/j.mio.2013.12.003

Sackmann, B., M. Perry, and C. Eriksen. 2008. Seaglider observations of variability in daytime fluorescence quenching of chlorophyll-a in Northeastern Pacific coastal waters. Biogeosci. Discuss. **5**: 2839–2865. doi:10.5194/bgd-5-2839-2008

Sauer, M. J., and C. S. Roesler. 2013. Unraveling phytoplankton optical variability in the Gulf of Maine during the spring and fall transition period. Cont. Shelf Res. **61**: 125–136. doi:10.1016/j.csr.2013.04.009

Sharples, J. 2007. Potential impacts of the spring-neap tidal cycle on shelf sea primary production. J. Plankton Res. **30**: 183–197. doi:10.1093/plankt/fbm088

Sharples, J., O. N. Ross, B. E. Scott, S. P. Greenstreet, and H. Fraser. 2006. Inter-annual variability in the timing of stratification and the spring bloom in the North-western North Sea. Cont. Shelf Res. **26**: 733–751. doi:10.1016/j.csr.2006.01.011

Simpson, J. H., J. Brown, J. Matthews, and G. Allen. 1990. Tidal straining, density currents, and stirring in the control of estuarine stratification. Estuaries **13**: 125–132. doi:10.2307/1351581

Simpson, J. H., and J. Sharples. 2012. Introduction to the physical and biological oceanography of shelf seas. Cambridge Univ. Press.

Sosik, H. M., S. W. Chisholm, and R. J. Olson. 1989. Chlorophyll fluorescence from single cells: Interpretation of flow cytometric signals. Limnol. Oceanogr. **34**: 1749–1761. doi:10.4319/lo.1989.34.8.1749

Sosik, H. M., and B. G. Mitchell. 1991. Absorption, fluorescence, and quantum yield for growth in nitrogen-limited *Dunaliella tertiolecta*. Limnol. Oceanogr. **36**: 910–921. doi:10.4319/lo.1991.36.5.0910

Sournia, A. 1975. Circadian periodicities in natural populations of marine phytoplankton. Adv. Mar. Biol. **12**: 325–389. doi:10.1016/S0065-2881(08)60460-5

Snyder, J., E. Boss, R. Weatherbee, A. C. Thomas, D. Brady, and C. Newell. 2017. Oyster Aquaculture Site Selection Using Landsat 8-Derived Sea Surface Temperature, Turbidity, and Chlorophyll a. Frontiers Mar. Sci. **4**: 190. doi:10.3389/fmars.2017.00190

Townsend, D. W., and others. 2015. Water masses and nutrient sources to the Gulf of Maine. J. Mar. Res. **73**: 93–122. doi:10.1357/002224015815848811

Werdell, P. J., and S. W. Bailey. 2005. An improved in-situ bio-optical data set for ocean color algorithm development and satellite data product validation. Remote Sens. Environ. **98**: 122–140. doi:10.1016/j.rse.2005.07.001

Wolovick, M. J. 2009. Density-driven subtidal circulation in eastern Casco Bay and its effects on Alexandrium blooms. Bowdoin College Honors Thesis, 70 pp.

Xing, X., and others. 2012. Quenching correction for in vivo chlorophyll fluorescence acquired by autonomous platforms: A case study with instrumented elephant seals in the Kerguelen region (Southern Ocean). Limnol. Oceanogr.: Methods **10**: 483–495. doi:10.4319/lom.2012.10.483

Conflict of Interest

None declared.